Cardiovascular Research
doi:10.1093/cvr/cvx020

Functional local crosstalk of inositol 1,4,5-trisphosphate receptor- and ryanodine receptor-dependent Ca^{2+} release in atrial cardiomyocytes

Marcel Wullschleger, Joaquim Blanch, and Marcel Egger*

Department of Physiology, University of Bern, Buehlplatz 5, CH 3012 Bern, Switzerland

Received 1 June 2016; revised 11 November 2016; editorial decision 18 January 2017; accepted 31 January 2017

Time for primary review: 50 days

Aims Enhanced inositol 1,4,5-trisphosphate receptor ($InsP_3R2$) expression has been associated with a variety of proarrhythmogenic cardiac disorders. The functional interaction between the two major Ca^{2+} release mechanisms in cardiomyocytes, Ca^{2+} release mediated by ryanodine receptors (RyR2s) and $InsP_3$-induced intracellular Ca^{2+} release (IP3ICR) remains enigmatic. We aimed at identifying characterizing local IP3ICR events, and elucidating functional local crosstalk mechanisms between cardiac $InsP_3R2$s and RyR2s under conditions of enhanced cardiac specific $InsP_3R2$ activity.

Methods and results Using confocal imaging and two-dimensional spark analysis, we demonstrate in atrial myocytes (mouse model cardiac specific overexpressing $InsP_3R2$s) that local Ca^{2+} release through $InsP_3Rs$ (Ca^{2+} puff) directly activates RyRs and triggers elementary Ca^{2+} release events (Ca^{2+} sparks). In the presence of increased intracellular $InsP_3$ concentrations IP3ICR can modulate RyRs openings and Ca^{2+} spark probability. We show as well that IP3ICR remains under local control of Ca^{2+} release through RyRs.

Conclusions Our results support the concept of bidirectional interaction between RyRs and $InsP_3Rs$ (i.e. Ca^{2+} sparks and Ca^{2+} puffs) in atrial myocytes. We conclude that highly efficient $InsP_3$ dependent SR-Ca^{2+} flux constitute the main mechanism of functional crosstalk between $InsP_3Rs$ and RyRs resulting in more Ca^{2+} sensitized RyRs to trigger subsequent Ca^{2+}-induced Ca^{2+} release activation. In this way, bidirectional local interaction of both SR-Ca^{2+} release channels may contribute to the shaping of global Ca^{2+} transients and thereby to contractility in cardiac myocytes.

Keywords $InsP_3R$ • RyR • Ca^{2+} sparks • Ca^{2+} puffs • CICR • Atrial myocytes • Local modulation of calcium sparks and calcium puffs

source: https://doi.org/10.7892/boris

Introduction

Ca^{2+}-induced Ca^{2+} release (CICR) is known as the main mechanism involved in the excitation–contraction coupling (ECC) of cardiomyocytes.[1] However a second mechanism involving $InsP_3$-induced intracellular Ca^{2+} release (IP3ICR) has been described.[2–4] It can be activated through the binding of cardioactive hormones to G protein–coupled receptors (GPCRs), amongst others endothelin-1 (ET-1) and angiotensin II (AngII). The contribution of IP3ICR to the CICR and therefore to the ECC in both normal and pathophysiological conditions remains poorly understood.

In atrial cardiomyocytes, the ryanodine receptors (RyRs) constitute the major mediator of SR-Ca^{2+} release. They are functionally coupled and organized in channel clusters.[5] The opening of these clustered RyRs, triggered by the Ca^{2+} influx through the voltage-operated L-Type Ca^{2+} channels, elicit local Ca^{2+} release events known as 'Ca^{2+} sparks', the basis for global Ca^{2+} transients.[6] The coordinated openings of clustered $InsP_3Rs$ will result, as well, in local SR-Ca^{2+} release called 'Ca^{2+} puffs' exhibiting distinct spatio-temporal properties.[7] In addition to microscopically detectable Ca^{2+} puffs, eventless SR-Ca^{2+} release by individual $InsP_3Rs$ openings has been described.[8]

Although the functional expression of $InsP_3Rs$ in cardiac tissue is limited, in comparison to RyRs, evidence suggests that the IP3ICR may contribute to the ECC in atrial cardiomyocytes.[9,10] This hypothesis is for instance, supported by the following observations: (i) under pathophysiological conditions the $InsP_3R$ expression is upregulated which

* Corresponding author. Tel: +41 31 631 8737, E-mail: egger@pyl.unibe.ch

Published on behalf of the European Society of Cardiology. All rights reserved. © The Author 2017. For Permissions, please email: journals.permissions@oup.com.

favours delayed afterdepolarizations and Ca^{2+}-dependent arrhythmogenicity[2,4]; (ii) down-regulation of $InsP_3Rs$ in cardiac tissue was found to be protective against pro-arrhythmogenic stress[11]; and (iii) small and invisible SR-Ca^{2+} release events originating from $InsP_3Rs$ openings were found to have a modulatory function on Ca^{2+} signalling in subcellular microdomains and may be involved in the functional crosstalk between RyRs and $InsP_3Rs$.[8]

The present study focuses on local functional crosstalk between IP3ICR and RyRs and aims at better understanding its impact on local Ca^{2+} release within atrial cardiomyocytes. Since a potential crosstalk between $InsP_3Rs$ and RyRs can only be investigated with high accuracy at a local scale with a substantial $InsP_3Rs$ activity, we opted to use an $InsP_3Rs$ transgenic mouse model[12] in which increased open probability (e.g. Ca^{2+} puffs) is a consequence of enhanced $InsP_3R$ expression. The transgenic (TG) model mimics a pathophysiological condition associated with both receptor alteration and increased $InsP_3R$ protein expression.[13–15] We examined local IP3ICR activity using a custom designed two-dimensional spark analysis algorithm and found that local IP3ICR events (Ca^{2+} puffs) in close proximity to RyRs lead to the activation of RyRs followed by CICR events (Ca^{2+} sparks). In addition, we found that the opposite direction of crosstalk seems to be possible: IP3ICR can be modulated by local Ca^{2+} release produced by RyRs. These results support the concept that IP3ICR, in a pathophysiological condition with increased $InsP_3Rs$ functional expression, may interfere with RyRs openings and Ca^{2+} spark probability in cardiac myocytes.

Methods

Cell preparation and chemicals

The $InsP_3R$ type II overexpressing mouse model[12] (TG) and WT (FVB/N background) mice were obtained from Charles River Laboratories (Germany). C57BL6 mice were provided by our Central Animal Facility, University of Bern (Switzerland) for control purposes. Hearts were removed after animals were euthanized by cervical dislocation. Acute atrial myocytes isolation was performed using the Langendorff perfusion technique. All experiments were performed at room temperature and approved by the State Veterinary Office of Bern, Switzerland, according to Swiss Federal Animal Protection Law (see Supplementary material online, *Figure S1*).

Pharmacological experiments included 2-aminoethoxydiphenyl borate (2-APB; Sigma-Aldrich), tetracaine (Sigma-Aldrich), xestospongin C (A.G. Scientific Inc.), $InsP_3$ AM (SiChem GmbH), endothelin-1 (ET-1; Sigma-Aldrich), DM-nitrophen AM (Setareh Biotech), phenylephrine hydrochloride (PE, Sigma-Aldrich), U-73122 and U-73343 (Tocris Bioscience). For Ca^{2+} imaging, atrial myocytes were incubated with Fluo-3 AM (Biotium), plated on ECM gel (Sigma-Aldrich) coated glass coverslips and further superfused with an extracellular solution containing (in mmol/L): 140 NaCl, 5 KCl, 1 $MgCl_2$, 1 Na_2HPO_4, 5 Hepes, 10 D-glucose; pH 7.4 (adjusted with NaOH) supplemented with 1.8 mmol/L Ca^{2+}.

Confocal Ca^{2+} imaging and data analysis

Rapid two-dimensional confocal full-frame Ca^{2+} imaging (150 Hz; 0.267 µm × 0.267 µm $pixel^{-1}$, 512 × 64 pixel per frame-scan) was performed on Fluo-3 AM loaded atrial myocytes using a diode laser (488 nm, 50 mW) and a multi-beam confocal scanner (VT-infinity, VisiTech international) mounted on an inverted microscope (Nikon). Raw data were initially analysed for frequency, mean fluorescence amplitude ($\Delta F/F_0$) and mean full width at half maximal amplitude in x- and y-direction ($FWHM_{x,y}$) using a two-dimensional Ca^{2+} spark analysis software.[16] A detailed event analysis was built using a python algorithm following a two-step pixel clustering procedure (density-based spatial clustering of applications with noise).[17] Ca^{2+} puff identification was performed by pharmacological separation and framescan (x-y-t) data. Local, immobile Ca^{2+} release events with a full duration at half maximal amplitude (FDHM) ≧ 180 ms and $(\Delta F/F_0 10^3)$/FDHM [ms] ≦ 3 were classified as Ca^{2+} puffs (the second condition was introduced in order to exclude 'macro-sparks'; see Supplementary material online for details). Data are presented as Tukey box-plots or mean [+/- standard deviation (SD)] values. Statistical comparison was performed as indicated within the figure legends as well as online supplementary materials. The number of animals (N), cells (n_c), and Ca^{2+} release events (n_e) are given in each of the figure legend.

Immunocytochemistry

For immunostaining cells were incubated overnight at +4 °C with a mix of primary antibodies against $InsP_3R2$ (1:1000, Abcam ab77838) and RyR2 (1:200, Abcam ab2827) followed by incubation with a mix of secondary anti-mouse and anti-rabbit antibodies conjugated to Alexa Fluor 488 and 568, respectively (1:600, Molecular Probes). For Western Blot anti-$InsP_3R2$ antibody (1:5000, KM1083, gift from Dr. K. Mikoshiba) or anti-GAPDH antibody (1:100 000, Fitzgerald 10R-G109A) was used. RT-qPCR was performed with primers specific for itpr2 and β-actin with the Eco Real-Time PCR system (Illumina) and using KAPA SYBR FAST One-Step kit (Kapa Biosystems).

A more detailed version of the method section is provided in the supplementary section.

Results

ET-1 induced $InsP_3R$ Ca^{2+} release in atrial myocytes

Figure 1 shows that rapid superfusion of atrial myocytes isolated from WT (FVB) mice with 100 nmol/L ET-1 caused an increase in spontaneous local Ca^{2+} release events of approximately 85% in comparison with control condition. This increase in local Ca^{2+} release events was completely antagonized by the $InsP_3R$ blocker xestospongin C (5 µmol/L). RyR2 inhibition (1 mmol/L tetracaine) in combination with ET-1 stimulation reduced the Ca^{2+} release frequency by 21% compared to control. This remaining Ca^{2+} event activity could be linked to IP3ICR activity. In atrial myocytes isolated from TGs overexpressing the $InsP_3R$ type II, stimulation with ET-1 triggered a more pronounced increase in local Ca^{2+} release of about 313% compared to control condition. This increase was antagonized by xestospongin C to values about 54% of control value. Tetracaine reduced as well the spontaneous local Ca^{2+} release events but down to 12% of control value.

Immunostaining of $InsP_3R2$s and RyR2s revealed a co-localization of $InsP_3R2$ with RyR2, suggesting a junctional and non-junctional distribution pattern for RyR2s and $InsP_3R2$s in atrial myocytes isolated from TG mice with cardiac specific overexpression of $InsP_3R2$s (see Supplementary material online, *Figure S1*). Semi-quantitative assessment for $InsP_3R2$ protein expression and RT-qPCR analysis determined a 1.6-fold increase in $InsP_3R2$s expression in TG mice compared to atrial tissue extracts from control.

To get further insight in the local contribution of IP3ICR and ensure the proper discrimination of CICR- and IP3ICR events, interventions aiming at controlling the phospholipase C (PLC) function were used. Atrial myocytes isolated from TGs were field-stimulated to control SR-Ca^{2+} loading conditions. The frequency of Ca^{2+} sparks, mini-waves (Ca^{2+} events propagating partially throughout the entire cell), and waves

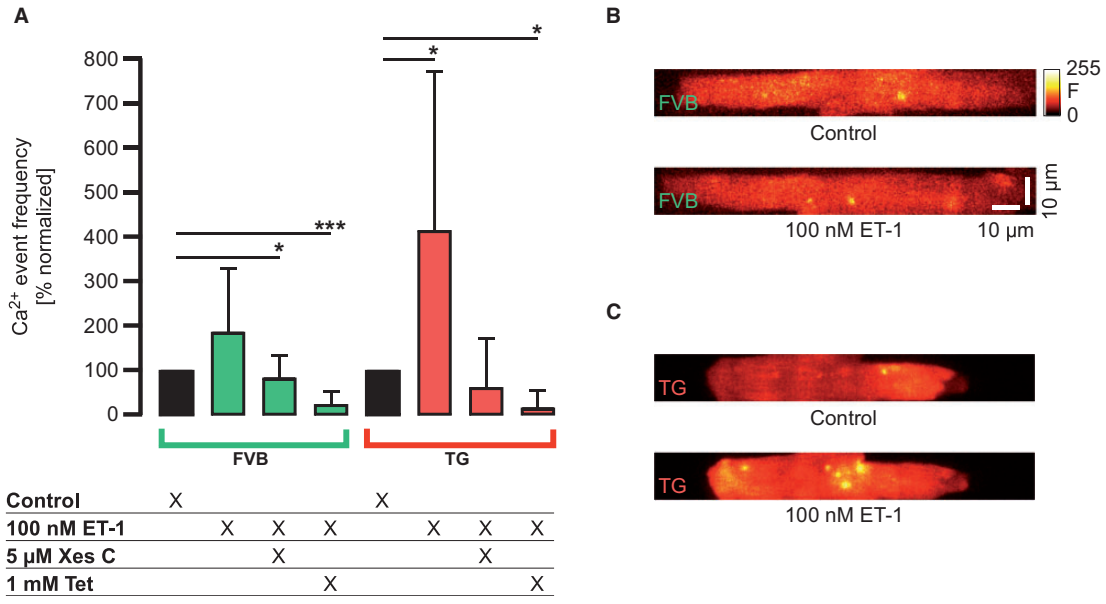

Figure 1 ET-1 increases Ca^{2+} release event occurrence. (*A*) Ca^{2+} event frequency normalized to spontaneous Ca^{2+} event frequencies in atrial myocytes obtained from FVB and TGs. Event frequency measured as Ca^{2+} sparks 10^3 $\mu m^{-2}s^{-1}$ in the presence of ET-1: FVB = 1.3 ($P = 0.102$), $n_c = 15$, $N = 4$; TGs = 9.0 ($P = 0.039$), $n_c = 8$, $N = 2$; ET-1 + xestospongin C: FVB = 2.6 ($P = 0.023$), $n_c = 15$, $N = 2$; TGs = 2.5 ($P = 0.255$), $n_c = 10$, $N = 2$; ET-1 + tetracaine: FVB = 0.2 ($P < 0.001$), $n_c = 33$, $N = 5$; TGs = 0.05 ($P = 0.016$) $n_c = 13$, $N = 2$. Histogram shows mean (SD) values. Groups were compared with a paired Student's *t*-test (*$P < 0.050$, **$P < 0.010$, ***$P < 0.001$). (*B* and *C*) Examples for spontaneous local Ca^{2+} events. Two framescan series were recorded from each cell (control vs. pharmacological intervention).

(Ca^{2+} events propagating throughout the entire cell) was measured upon specific pharmacological intervention (*Figure 2B*). In comparison to control condition, application of 10 µmol/L of the α_1-adrenergic receptor agonist phenylephrine (PE) increased Ca^{2+} spark frequency per confocal recording area by 152% from 3.4 (4.0 SD) to 5.1 (3.6 SD) 10^3 $\mu m^{-2}s^{-1}$ ($n_c = 8$; *Figure 2C*). In the presence of 1 µmol/L U-73122 (PLC inhibitor), the observed PE increased Ca^{2+} spark frequency was absent. The inactive PLC inhibitor analogue U-73343 (1 µmol/L) failed to alter the PE effect with an increased Ca^{2+} spark frequency by 283% upon PE administration from 1.8 (1.9 SD) to 5.1 (4.0 SD) events 10^3 $\mu m^{-2}s^{-1}$. The frequency of Ca^{2+} mini-waves increased from 1.5 (2.3 SD) to 2.4 (4.8 SD) events 10^3 $\mu m^{-2}s^{-1}$, whereas the Ca^{2+} wave occurrence decreased from 0.3 (0.3 SD) to 0.0 (0.0 SD) events $cell^{-1}s^{-1}$. Concomitant inhibition of PLC (1 µmol/L U-73122) and in combination with RyR2 inhibition (1 mmol/L tetracaine) led to the absence of any event while in the presence of both 1 µmol/L U-73343 and 1 mmol/L tetracaine, Ca^{2+} sparks and Ca^{2+} mini-waves were reduced to a frequency with very rare events (*Figure 2D*).

Taken together, these observations support that in atrial myocytes ET-1 receptor stimulation subsequently triggered Ca^{2+} release events which may be caused, at least in part, by IP3ICR. In addition, intracellular provision of $InsP_3$ in terms of PLC activation (e.g. induced by a humoral agonist) appears to be a precondition for IP3ICR. An increased number of $InsP_3$ dependent Ca^{2+} events in cells from TGs may facilitate the probability of potential crosstalk events between $InsP_3$Rs and RyRs. These interactions can accurately be examined on a local scale exclusively with an appropriate basal $InsP_3$Rs activity.

As illustrated in *Figure 3*, we analysed the amplitude ($\Delta F/F_0$), $FWHM_x$, and $FWHM_y$ of individual Ca^{2+} events by using conventional two-dimensional Ca^{2+} spark analysis tools. The spatio-temporal characterization of ET-1 triggered Ca^{2+} events in atrial myocytes isolated from FVB and TG mice did not reveal distinct classes of events (i.e. Ca^{2+} sparks and Ca^{2+} puffs), even though we would have expected for one group increased $FWHM_{x,y}$ and smaller $\Delta F/F_0$, due to 'Ca^{2+} puffs'. Nevertheless, in the presence of RyR inhibition by tetracaine the remaining Ca^{2+} release events showed a smaller amplitude, suggesting a small proportion of possibly $InsP_3$-induced Ca^{2+} release events in atrial myocytes. Local Ca^{2+} release events were also assessed in permeabilized atrial myocytes using classical confocal linescan mode (see Supplementary material online, *Figure S2*). Compared to control condition, superfusion with the RyR antagonist tetracaine (1 mmol/L) abolished detectable Ca^{2+} release events, whereas subsequent selective stimulation of $InsP_3$Rs (20 µmol/L $InsP_3$-salt, 1 mmol/L tetracaine) partially recovered Ca^{2+} release event activity. This persistent Ca^{2+} event activity was sensitive to the $InsP_3$R antagonist 2-APB (2 µmol/L) with previously triggered Ca^{2+} release events being suppressed. Spatio-temporal characterization of these events showed overlap with control, but a fraction of events was found to be lower in amplitude and longer in FDHM, supporting that IP3ICR contributes at least in part to the total number of Ca^{2+} events (see supplementary material online).

Taken together and based on the pharmacological interventions, IP3ICR appears to contribute to the constitution of local Ca^{2+} release events, although their spatio-temporal characterization by using conventional two-dimensional or one-dimensional Ca^{2+} spark analysis fails to

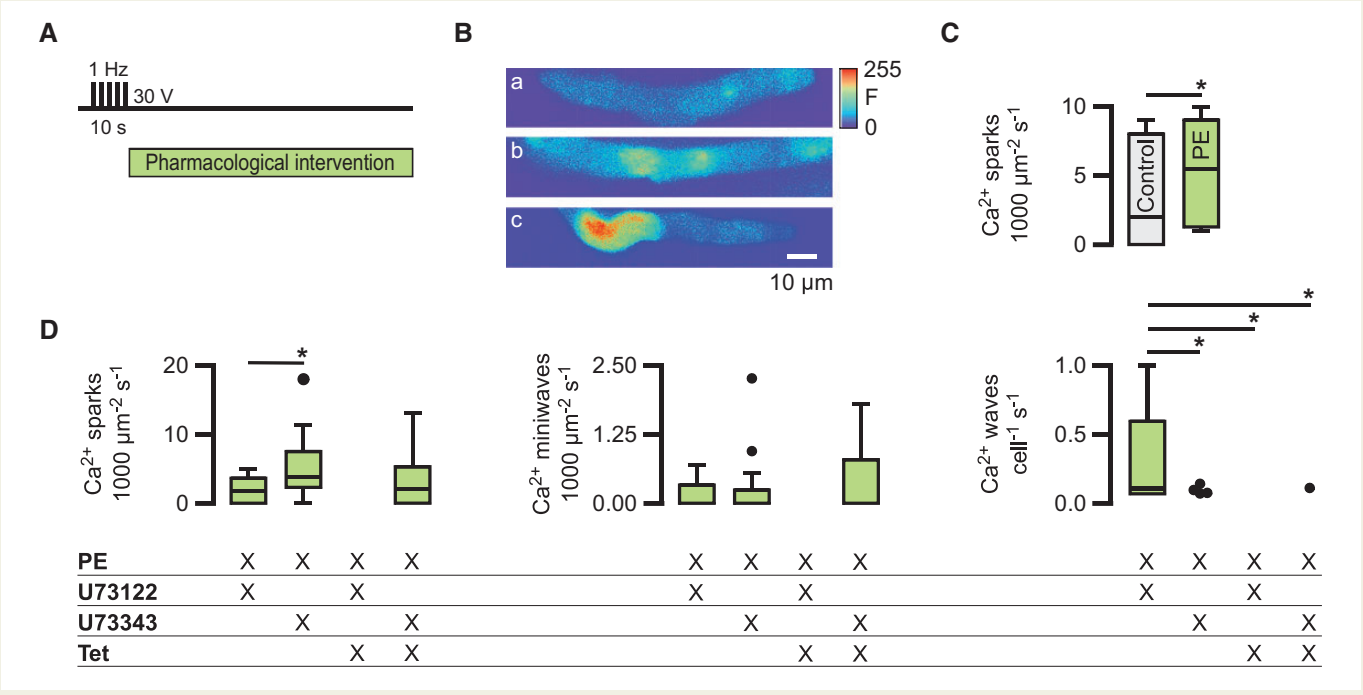

Figure 2 Inhibition of the $InsP_3$ signalling pathway reduces Ca^{2+} event occurrence in $InsP_3R2$ TGs. (*A*) Experimental protocol; (*B*) Spontaneous local Ca^{2+} sparks (a), Ca^{2+} mini-waves (b), and Ca^{2+} waves (c) in the presence of PE (10 µmol/L), which leads to an increase in Ca^{2+} spark frequency compared to control conditions ($P = 0.026$; *C*). (*D*) Ca^{2+} event frequency (Ca^{2+} sparks, Ca^{2+} mini-waves, Ca^{2+} waves) in the presence PE (10 µmol/L) in combination with: PLC inhibitor U-73122 (1 µmol/L), inactive analogue PLC inhibitor U-73343 (1 µmol/L) and tetracaine (Tet; 1 mmol/L). Left: Ca^{2+} spark frequency is reduced (PE, U-73122, $P = 0.021$). Tet reduces Ca^{2+} sparks partially (PE, U-73343, Tet; $P = 0.934$) or completely (PE, U-73122, Tet; $P = 0.155$). Middle: For Ca^{2+} mini-waves, the median value for each group is found to be 0. Some samples exhibit Ca^{2+} mini-waves, e.g. when RyR2s are blocked. For the third group (PE, U-73122, Tet) no Ca^{2+} mini-waves are identified ($P = 0.213$). Right: Ca^{2+} waves in the presence of PE and U-73122; Ca^{2+} wave frequency are statistically significant compared to each of the other groups, $P < 0.001$). n_c (Group 1–4) = 13,25,10,18; $N = 6,2,1,4$. Data are presented as Tukey boxplots with median values (see Supplementary material). For multiple comparison, a Kruskal–Wallis test was applied (non-normally distributed data; $*P < 0.050$, $**P < 0.010$, and $***P < 0.001$).

clearly identify the expected two distinct classes of events corresponding to Ca^{2+} sparks and Ca^{2+} puffs.

The discrepancy between pharmacological identification and separation of events (e.g. Ca^{2+} sparks/Ca^{2+} puffs) on an individual scale using their spatio-temporal profile was unexpected and limits future detailed mechanistic studies of functional crosstalk between RyRs and $InsP_3Rs$.

Identification and separation of individual Ca^{2+} puffs and Ca^{2+} sparks

To overcome the limitations mentioned above, we applied a custom-made mathematical tool to analyse local Ca^{2+} release events with an individual pixel basis applied on mapped regions of interest (ROIs) of two-dimensional full-frame confocal image stacks (*Figure 4*).[17]

Each pixel is characterized by various individual parameters (amplitude, duration, τ_{rise}, τ_{decay}) which together determine the shape of each Ca^{2+} release event. In order to characterize a pixel event, the pixel's location in space and time should be known as well. In other words, a pixel event can be completely defined by two vectors: the shape vector and the position vector. If done, a new 'denoised' event-image can be reconstructed. However, a prior two-step clustering procedure of pixels needs to be performed (density-based spatial clustering of applications with noise).[18] A first clustering of pixels according to their shape is then followed by a spatio-temporal clustering within that group. The outcome then allows the extraction of desired parameters from the cluster such as amplitude, FDHM, $FWHM_{x,y}$, rise and decay times and separation into physiologically relevant Ca^{2+} signalling events (e.g. Ca^{2+} sparks/Ca^{2+} puffs).

As aforementioned, the procedure started with a conventional Ca^{2+} spark analysis where local Ca^{2+} release events were first detected.[19] Selected single Ca^{2+} release events were further processed for a detailed analysis using our pixel-wise fitting algorithm, whereby the fitted fluorescence intensity fluctuation within each pixel, belonging to the ROI and a selected time window, were clustered according to the combined spatio-temporal characteristics: amplitude, τ_{rise}, FDHM, τ_{decay}, $FWHM_x$, and $FWHM_y$ (level 'Ca^{2+} release event'). Pixel intensities for each ROI were calculated to establish threshold values for Ca^{2+} puffs (FDHM $\geqq$ 180 ms *and* $(\Delta F/F_0 10^3)$/FDHM [ms] $\leqq$ 3) and thus provide the basis for analysis of the two-dimensional full-frame image stacks.

One advantage of this procedure is, that even though the spatio-temporal characteristics of pixels (individual parameters) within the ROI are not statistically different, the combination of all the obtained parameters will ensure the success in providing an optimal event separation. The core of local Ca^{2+} release events can thus be precisely determined, facilitating the exclusion of Ca^{2+} mini-waves and fuzzy signals due to Ca^{2+} diffusion. *Figure 4A–C* shows a confocal frame-scan image of an atrial myocyte exhibiting a Ca^{2+} spark and a Ca^{2+} puff. In this example,

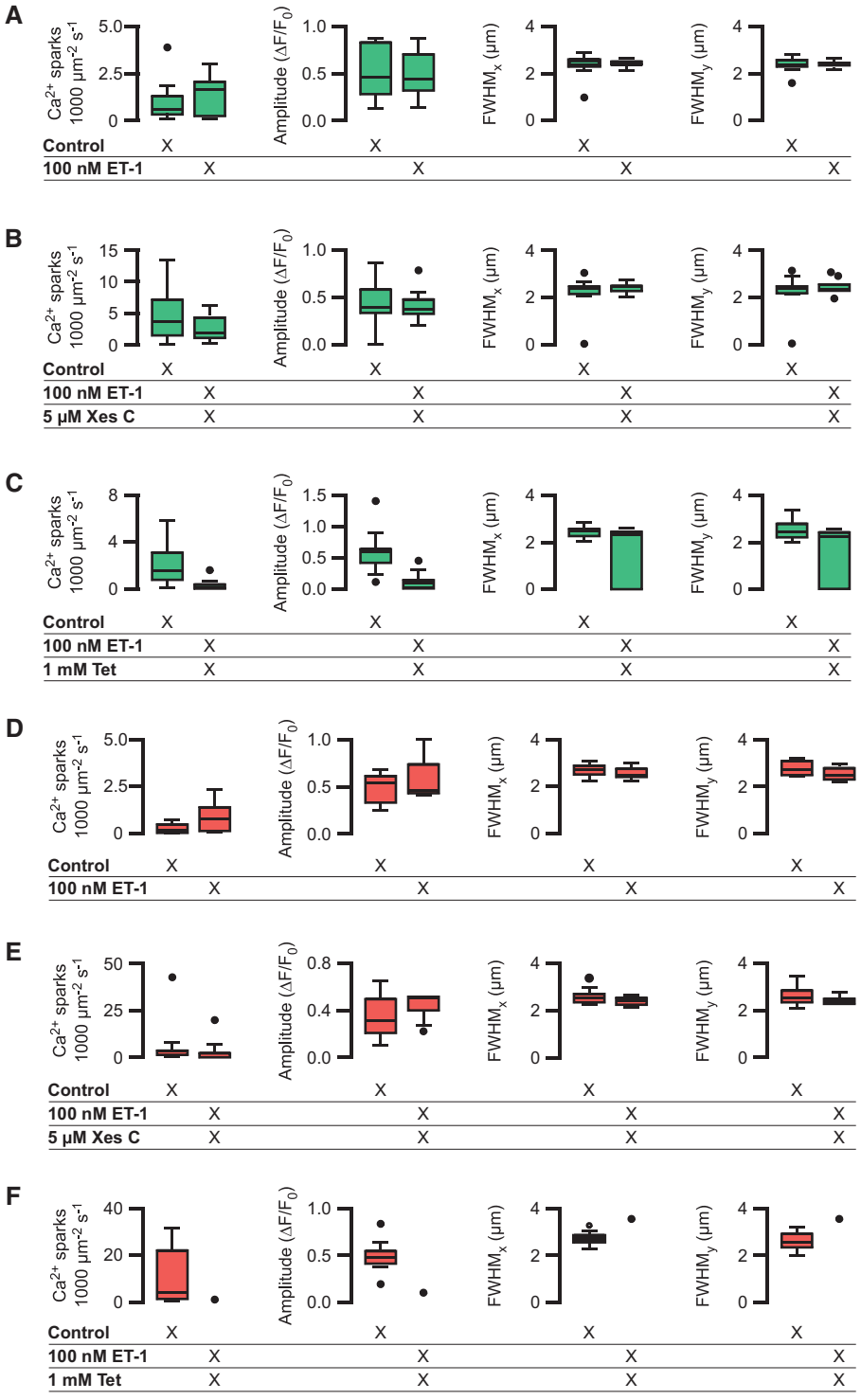

Figure 3 ET-1 induced SR-Ca^{2+} release in atrial myocytes. Spatio-temporal characterization of local Ca^{2+} events by using conventional two-dimensional Ca^{2+} spark analysis fails to identify two distinct classes of events such as Ca^{2+} sparks and Ca^{2+} puffs. (*A*) ET-1 (100 nmol/L; $n_c = 15$, $N = 4$): Ca^{2+} spark frequency (1.34 Ca^{2+} sparks 10^3 $\mu m^{-2} s^{-1}$, $P = 0.104$), $\Delta F/F_0$ ($P = 0.828$), $FWHM_x$ ($P = 0.600$), $FWHM_y$ ($P = 0.561$); (*B*) ET-1 + xestospongin C (5 µmol/L; $n_c = 15$, $N = 2$): Ca^{2+} spark frequency ($P = 0.023$), $\Delta F/F_0$ ($P = 0.092$), $FWHM_x$ ($P = 0.561$), and $FWHM_y$ ($P = 0.720$); (*C*) ET-1 + tetracaine (1 mmol/L; $n_c = 33$, $N = 5$): Ca^{2+} event frequency ($P < 0.001$), $\Delta F/F_0$ ($P < 0.001$), $FWHM_x$ ($P < 0.001$) and $FWHM_y$ ($P < 0.001$). (*D*) ET-1 ($n_c = 8$, $N = 2$): Ca^{2+} spark frequency ($P = 0.039$). $\Delta F/F_0$ ($P = 0.251$), $FWHM_x$ ($P = 0.358$), and $FWHM_y$ ($P = 0.055$); (*E*) ET-1 + xestospongin C ($n_c = 10$, $N = 2$): Ca^{2+} spark frequency ($P = 0.266$), $\Delta F/F_0$ ($P = 0.618$), $FWHM_x$ ($P = 0.220$), and $FWHM_y$ ($P = 0.292$). (*F*) ET-1 + tetracaine ($n_c = 13$, $N = 2$) is followed by an almost complete elimination of detected Ca^{2+} release events ($P = 0.016$). Data are presented as Tukey boxplots with median values. For normally distributed data a two-tailed, paired Student's *t*-test was applied. Non-normally distributed samples were evaluated with the Wilcoxon matched-pairs signed rank test. Analysis of variance was used for samples with unequal numbers of data records.

the time course of averaged F/F_o fluorescence intensity is taken from pseudo-linescan (linescan-type x-t plot from a x-y-t timecourse) analysis. The ROIs shown include a Ca^{2+} spark and a Ca^{2+} puff. The maximal signal of each pixel in the ROI illustrated in *Figure 4C* allows the clustering of events (*Figure 4D*). Even though, pixels exhibit some overlap in the cluster of F/F_o fluorescence and/or other parameters (e.g. FDHM), Ca^{2+} sparks and Ca^{2+} puffs can be distinguished. The threshold used for Ca^{2+} puff classification is illustrated in *Figure 4E*. *Figure 4F* and *G* shows a typical Ca^{2+} spark and Ca^{2+} puff- separation and -classification based on the spatio-temporal parameters. Numerical data of the same example are given in the supplements (see Supplementary material online, *Table S1*). Spatio-temporal parameters were found to be statistically significant with the exception of $FWHM_x$ and $FWHM_y$.

Figure 5 shows representative spatio-temporal parameters obtained for Ca^{2+} puffs ($n_e = 95$; *Figure 4F* and *G*) from atrial myocytes isolated from FVB and TG mice. No significant differences in the Ca^{2+} event characteristics were observed. In addition, no differences were found in classified Ca^{2+} puffs from C57BL6 atrial myocytes. *Figure 5* shows, as well, that the spatio-temporal profile of Ca^{2+} puffs are independent from their trigger (e.g. ET-1, $InsP_3$ AM). Of importance, the spatio-temporal profile of the classified Ca^{2+} puffs is not significantly affected by tetracaine RyR inhibition. This supports the robustness of our approach.

In conclusion, the pixel-wise fitting algorithm approach in combination with a Ca^{2+} puff thresholding and appropriate selective pharmacology allows a successful separation and classification of local Ca^{2+} release events.

RyR-Ca^{2+} release can be directly provoked by $InsP_3$R-Ca^{2+} release (Ca^{2+} puff vs. Ca^{2+} spark)

Because of the limited experimental accessibility on a local scale, the functional crosstalk of RyR and $InsP_3$R in cardiac myocytes was considered elusive. The approach described above enables a detailed functional characterization of local interactions between IP3ICR and CICR.

Although we are expecting a constitutive crosstalk between RyRs and $InsP_3$Rs (e.g. in FVB mice), the probability of interaction may be rather limited in control condition where the expression of $InsP_3$Rs is low. For this reason, our functional crosstalk studies were performed on cells isolated from TG mice where the IP3ICR event probability is higher.

Freshly isolated atrial myocytes from TG mice were treated with either 50 μmol/L $InsP_3$ AM, 100 nmol/L ET-1 or 10 μmol/L phenylephrine to increase the occurrence of IP3ICR events. Ca^{2+} release event sites (e.g. showing a Ca^{2+} puff) were further identified. Occasionally, Ca^{2+} sparks were found close to regions of Ca^{2+} puffs ($n_e = 10$). *Figure 6A* and *B* illustrates a ROI exhibiting a Ca^{2+} spark with adjacent Ca^{2+} puff. Analysis of the event sequence suggested that the Ca^{2+} spark occurred subsequently to the Ca^{2+} puff but within the sustained time window and within the ROI (defined as 66 μm^2 with the Ca^{2+} puff in the centre). The mean delay between the interdependent sequences of Ca^{2+} puff and Ca^{2+} spark onsets was 266 ms (164 SD, $n_e = 10$; *Figure 6C*). From the total number of identified pair of events, the probability that these event sequences occurred spontaneously in a non-coordinated fashion was below 1% (see Supplementary material online, *Table S3*). This sequence of events was absent in the presence of the $InsP_3$R2 antagonist xestospongin C (5 μmol/L; $n_c = 12$) or the RyR2 blocker tetracaine (1 mmol/L; $n_c = 22$).

IP3ICR is sensitive to CICR

The open probability of the $InsP_3$R2 is known to be modulated by cytosolic and luminal $[Ca^{2+}]_i$.[20] Because of the spatial proximity of RyR2 and $InsP_3$R2 in atrial myocytes, we hypothesized that CICR may also directly affect the open probability of the $InsP_3$R2. For this reason, we transiently increased the Ca^{2+} spark frequency by ultraviolet (UV)-flash photolysis of caged Ca^{2+} (50 μmol/L DM-nitrophen AM) in the presence of high-intracellular $InsP_3$ (50 μmol/L $InsP_3$ AM).

Cells were conditioned by field stimulation. The frequency and local sequence of Ca^{2+} puffs as well as spontaneous Ca^{2+} sparks were examined (*Figure 7A–C*). In control conditions (high $[InsP_3]_i$), a Ca^{2+} puff/Ca^{2+} spark frequency ratio (f_P/f_S) of 0.022 was determined (f_P/f_S; 0.2 Ca^{2+} puffs 10^3 $\mu m^{-2}s^{-1}$, 9.2 Ca^{2+} sparks 10^3 $\mu m^{-2}s^{-1}$; $n_c = 8$). Before UV-flash photolysis of caged Ca^{2+} f_P/f_S ratio was 0.017 (0.1 Ca^{2+} puffs 10^3 $\mu m^{-2}s^{-1}$, 5.8 Ca^{2+} sparks 10^3 $\mu m^{-2}s^{-1}$; $n_c = 56$). The reduced Ca^{2+} spark frequency prior to photolytic Ca^{2+} release may be explained by a Ca^{2+} buffering action of DM-nitrophen. After a moderate but rapid photolytic $[Ca^{2+}]_i$ jump, the frequency of spontaneous Ca^{2+} sparks increased to 186%. This manoeuvre also increased the f_P/f_S ratio about two-fold ($f_P/f_S = 0.037$; 0.4 Ca^{2+} puffs 10^3 $\mu m^{-2}s^{-1}$, 10.8 Ca^{2+} sparks 10^3 $\mu m^{-2}s^{-1}$; $n_c = 56$, *Figure 7D*) suggesting that the Ca^{2+} puff frequency was affected by local CICR. Sequence analysis at a local scale revealed that IP3ICR events occurred subsequently to Ca^{2+} spark initiation with a delay of 49 ms (12 SD; *Figure 7E*) and with a probability of 9% (5/56). The probability of misclassification of the sequence (e.g. Ca^{2+} puffs arising randomly at the time of photolytic intracellular Ca^{2+} release) was found to be lower than 2% within a time window of 500 ms following $[Ca^{2+}]_i$ increase. The CICR to IP3ICR event sequence was not observed in the presence of 5 μmol/L xestospongin C ($n_c = 9$) and/or in combination with the RyR2 blocker tetracaine (1 mmol/L; $n_c = 6$).

Ca^{2+} release events occurring after rapid $[Ca^{2+}]_i$ increase are spatio-temporally identical to IP3ICR events under control conditions (see *Figure 7F*, see Supplementary material online, *Table S2*). Although, τ_{rise}, FDHM, τ_{decay}, $\Delta F/F_o$, and $FWHM_{x,y}$ were in the same order of magnitude, the mean FDHM (241 ms, 116 SD) was found to be shorter than the internal reference for FDHM (403 ms, 196 SD) for Ca^{2+} puffs. FDHM was longer than the typical range of Ca^{2+} sparks which averaged 61 ms (25 SD). With 0.3 (0.2 SD) $\Delta F/F_o$ the amplitude was in the lower range compared to previous data obtained, i.e. 0.4 (0.2 SD).

Discussion

The current observations unmask the existence of previously unrecognized functional bi-directional crosstalk of $InsP_3$R2 and RyR2 in atrial cardiomyocytes. Although this interaction has been suggested, the mechanisms have not yet been directly examined at a local subcellular scale.[2,21,22]

Identification of CICR and IP3ICR events in atrial myocytes

Recent studies have focused on the IP3ICR mechanism and its regulatory functions on CICR and excitation–transcription coupling (ETC) in cardiomyocytes.[15,23] In atrial myocytes, the central mechanism for ECC is the CICR. However, the significance of IP3ICR in initiation, propagation, and amplification of local and global SR-Ca^{2+} release in atrial myocytes remains open.[3] A direct impact of IP3ICR on ECC and ETC has been suggested. This idea was based on indirect functional studies including global

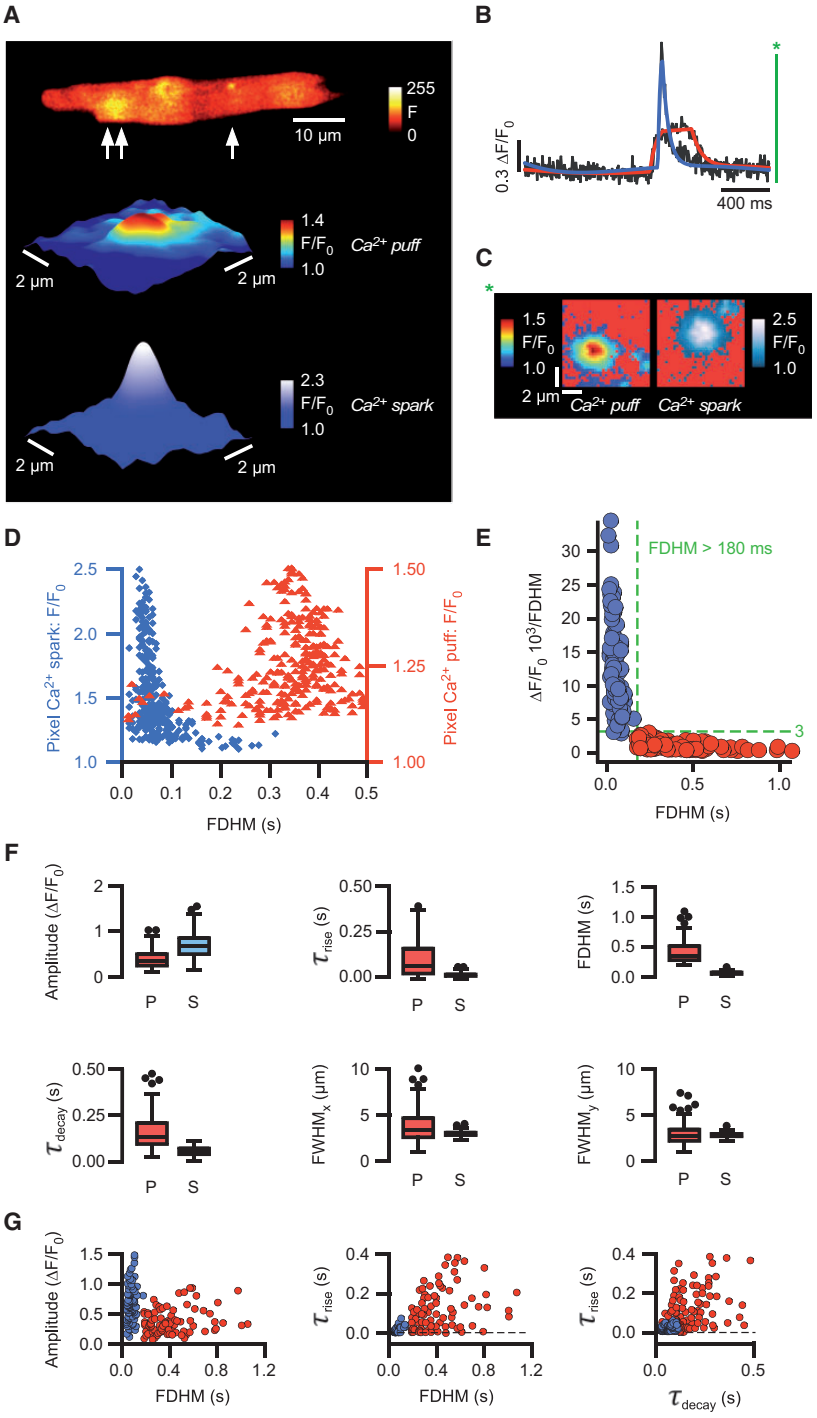

Figure 4 Identification of Ca^{2+} puffs and Ca^{2+} sparks. $InsP_3R_2$s in intact atrial myocytes were stimulated by ET-1 (100 nmol/L), PE (10 µmol/L), or directly with 50 µmol/L $InsP_3$ AM, RyRs were inhibited with tetracaine (1 mmol/L) in some measurements (for specification according pharmacological intervention/animal type (see *Figure 5* and see Supplementary material online, *Table S2*). (*A*) Spontaneous Ca^{2+} spark (single arrow) and Ca^{2+} puff (double arrow), (*B*) Time course of F/F_0 fluorescence of a Ca^{2+} spark (blue) and a Ca^{2+} puff (red) based on pseudo-linescans extracted from the image sequence. (*C*) Ca^{2+} puff and Ca^{2+} spark in the x-y-ROI can be identified (same events as shown in *B*). (*D*) Maximum fluorescence amplitude and FDHM for each pixel within the ROI are shown. The blue cloud refers to the Ca^{2+} spark, the red one to the Ca^{2+} puff. The overlap within the Ca^{2+} spark cloud is due to peripheral pixels of the Ca^{2+} puff showing similar values for amplitude and FDHM. (*E*) Boundary conditions for Ca^{2+} puff classification ($n_e = 95$). (*F*) Ca^{2+} puff (*P*; $n_e = 95$, $n_c = 74$, $N = 34$) and Ca^{2+} spark (S, $n_e = 95$, $n_c = 88$, $N = 30$) characteristics. Equal numbers of randomly selected Ca^{2+} sparks were used for comparison. Differences between Ca^{2+} puffs and Ca^{2+} sparks were statistically significant for amplitude ($P < 0.001$), τ_{rise} ($P < 0.001$), FDHM ($P < 0.001$), τ_{decay} ($P < 0.001$), and $FWHM_x$ ($P < 0.001$). $FWHM_y$ ($P = 0.679$) was not significant. (*G*) Distribution of Ca^{2+} puffs (red dots) and Ca^{2+} sparks (blue dots). Data are given as Tukey boxplots with median values, groups were compared by unpaired Student's *t*-test or a Mann–Whitney *U* test (non-normal distribution).

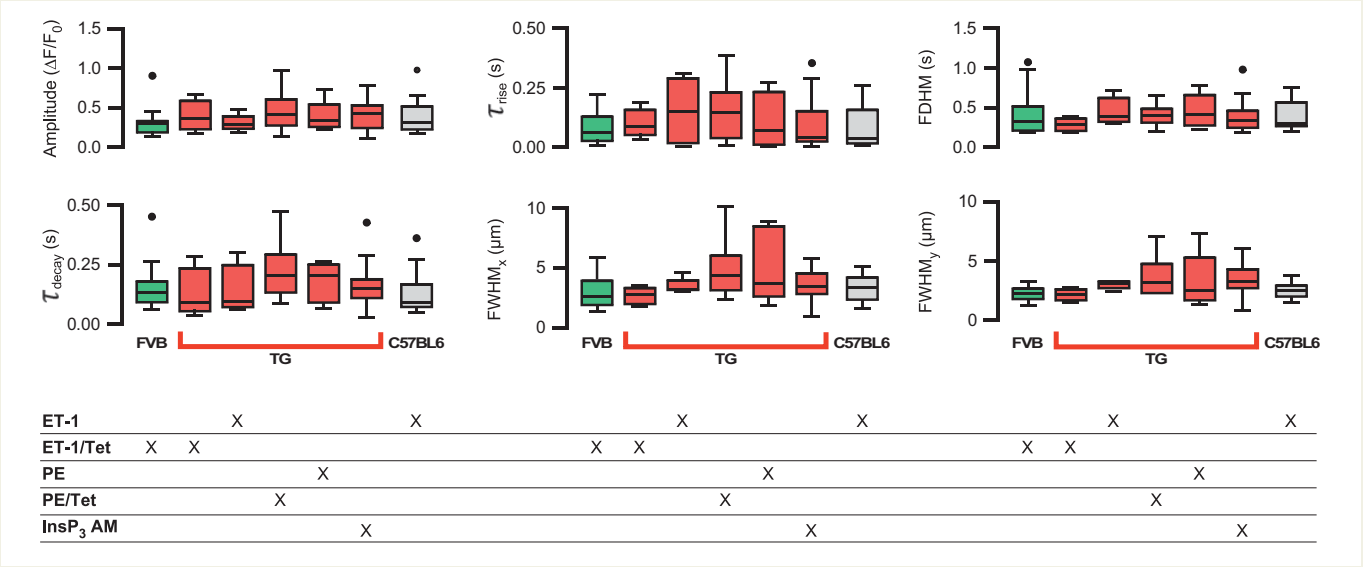

Figure 5 Spatio-temporal characterization of Ca^{2+} puffs under various pharmacological interventions and animal type. No significant differences for Ca^{2+} puffs under various conditions ($n_e = 95$; shown in *Figure 4*) and mouse models [FVB (WT), $InsP_3R$ TGs, C57BL6] were obtained. Stimulation of $InsP_3Rs$ and/or inhibition of RyRs was provoked by endothelin-1 (ET-1; 100 nmol/L), phenylephrine hydrochloride (PE; 10 µmol/L), $InsP_3$ AM (IP_3 AM; 50 µmol/L), and tetracaine (Tet; 1 mmol/L). Multiple comparisons (with FVB samples as control) did not show statistically significant differences except for TGs (PE + Tet) for amplitude ($P = 0.023$), $FWHM_x$ ($P = 0.005$), $FWHM_y$ ($P = 0.001$) and for TG (IP_3 AM) for $FWHM_y$ ($P = 0.026$). Data are presented as Tukey boxplot with median values. For multiple comparison, a Kruskal–Wallis test was applied. Corresponding mean (SD) data are given in Supplementary material online, *Table S2*.

and local SR-Ca^{2+} release, $InsP_3R$ expression, and immunohistochemistry.[2,21,22] TG mouse models have been rarely used because in mouse cardiomyocytes the direct detection of IP3ICR events was considered to be limited.[8,24]

We hypothesized that conventional Ca^{2+} spark analysis tools are not sensitive enough to allow the identification of Ca^{2+} puffs in cardiomyocytes with a sufficient precision, a statement based on one-dimensional confocal linescan analysis. The reason is that the probability of IP3ICR events is generally low in cardiac preparations.[9] In addition, Ca^{2+} puffs may not differ significantly in terms of their spatio-temporal profiles from other elementary Ca^{2+} release events. Importantly, pharmacological separation between Ca^{2+} puffs and Ca^{2+} sparks has some limitations due to incomplete specificity.[25] In our approach, full frame raw data were partitioned into specific ROIs and SOIs (sequences of interest, e.g. for the full duration of Ca^{2+} release events). ROI framescan series were subsequently processed by cluster analysis of Ca^{2+} events: density-based spatial clustering of applications with noise.[18] This multi-parametric approach enabled us to extract parameters such as amplitude, FDHM, FWHM, rise time, decay time, and to separate and classify Ca^{2+} puffs and Ca^{2+} sparks (*Figure 4D*). This approach is comparable to a multi-dimensional vector rotating in a data cloud, where the vector length and orientation depend on the value of each individual data point within the data cloud. It should be pointed out that even individual spatio-temporal parameters of pixels within the ROI may not be significantly different, but by combining different pixel parameters, the procedure may successfully find an optimum for event separation. In other words, by using a combination of all spatio-temporal event parameters, a differentiation and classification of events can be made. Even though parameters (e.g. $FWHM_y$) from both event types strongly overlapped when taken as individual parameter, in combination with others (e.g. $\Delta F/F_0$, τ_{rise}, τ_{decay}, FDHM) they were sufficient for event discrimination. For $\Delta F/F_0$ thresholds, 75% of Ca^{2+} puffs were found to be equal or below 0.5 ($\Delta F/F_0$) and about 25% of Ca^{2+} sparks were also found in this range. τ_{rise} and τ_{decay} were similar between Ca^{2+} puffs and sparks with values in the range of 70–110 ms. In case of Ca^{2+} puff separation, a discrimination threshold of 180 ms for FDHM was validated. Compared to Ca^{2+} sparks elicited by RyR2s, Ca^{2+} puffs have slower kinetics and show smaller amplitudes.[2,5] The obtained spatio-temporal profiles of Ca^{2+} sparks and Ca^{2+} puffs were comparable with previously published studies with different animal preparations (see Supplementary material online, *Table S1*).[5,26] The robustness of the applied approach was underscored by the key observation that the extraction of parameters (e.g. amplitude, FDHM, FWHM, rise-, decay -times etc.) from local events classified as 'Ca^{2+} puffs' were (i) independent from the source of preparation (FVB, TG's, C57BL6), (ii) not affected by the nature of the trigger inducing IP3ICR, and (iii) not affected by the RyR inhibitor tetracaine. Hence, the present study substantiates simultaneously occurring Ca^{2+} sparks and Ca^{2+} puffs in atrial cardiomyocytes.

Functional crosstalk between $InsP_3R2$ and RyR2

Functional modulation of RyR2s open probability and Ca^{2+} sensitivity by co-localized IP3ICR was originally conceptualized for smooth muscle cells. An increase in $[Ca^{2+}]_i$ through activity of $InsP_3Rs$ has been suggested to recruit neighbouring RyRs domains through increased $[Ca^{2+}]_i$ in the vicinity of RyRs. Such an effect triggers CICR as well as saltatory propagation of Ca^{2+} waves in the myocytes of the portal vein.[27] This concept is also in accordance with previous reports in adult cat

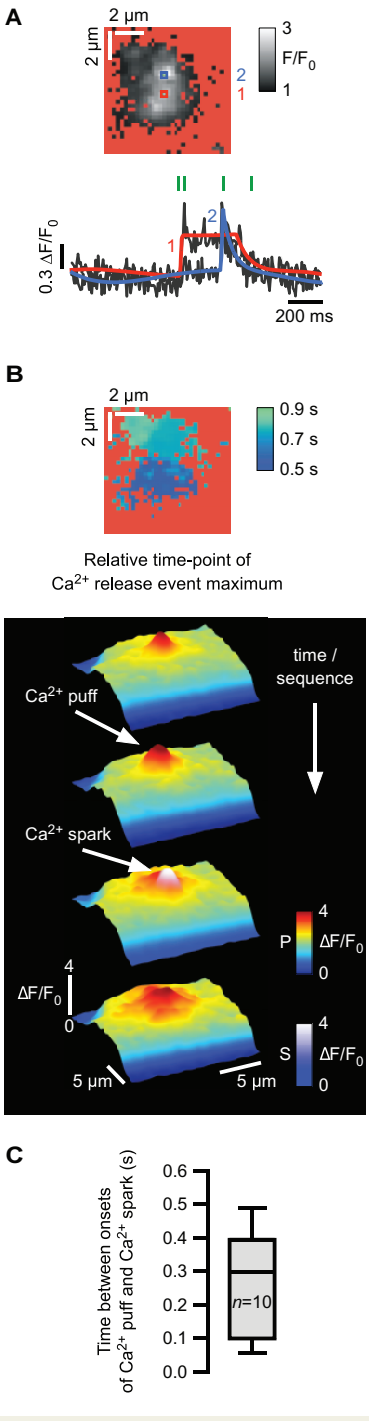

Figure 6 (*A*) Local IP3ICR with subsequently triggered Ca^{2+} sparks (CICR). The x-y-ROI shows an IP3ICR event with an adjacent Ca^{2+} spark. The corresponding time courses of fluorescence are given below, red: Ca^{2+} puff, blue: Ca^{2+} spark, green marks (I) correspond to the surface plots shown in B. (*B*) Time-coded mapping of a ROI (colour codes for the time-point of the Ca^{2+} release event maxima). The Ca^{2+} puff (dark blue area) occurred 584 ms after starting the SOI. The Ca^{2+} spark (green area) followed after another 210 ms, a second Ca^{2+} spark (lime area) after 869 ms from starting the SOI. Surface plot series of a Ca^{2+} puff triggering a Ca^{2+} spark. (*C*) The mean delay between the onsets of the Ca^{2+} puff and the Ca^{2+} spark was 266 ms (164 SD). Cells were treated either with $InsP_3$ AM (50 µmol/L), ET-1 (100 nmol/L), or PE (10 µmol/L). $n_e = 10$, $n_c = 9$, $N = 6$. Data are presented as Tukey boxplot with median value.

atrial myocytes[2] and rabbit ventricular myocytes.[28] The underlying mechanisms suggest enhanced RyR2 Ca^{2+} sensitivity with increased $[Ca^{2+}]_i$ through IP3ICR.[29]

So far, elucidating cardiac $InsP_3Rs$/RyRs crosstalk mechanisms was largely limited to observations on the level of global Ca^{2+} events (e.g. of Ca^{2+} waves or Ca^{2+} transients) or by an indirect proof of interaction quantifying the modulation of Ca^{2+} event frequencies.[30] The observation of individual Ca^{2+} sparks triggered by individual IP3ICR events in cardiomyocytes has not been reported before, although previous studies have mentioned a contribution of IP3ICR to local Ca^{2+} signalling.[3] The immunofluorescent determination of RyR2 and $InsP_3R2$ co-localization in our TG model supports the observed functional crosstalk of the two SR-Ca^{2+} release channels. Recently, we reported that 'eventless' IP3ICR, which do not go along with Ca^{2+} puffs, could also favour CICR.[8] In the present study, we confirm this hypothesis with a direct identification of Ca^{2+} puffs causing Ca^{2+} sparks.

We suggest that $InsP_3Rs$ open probability, which at least could lead to different Ca^{2+} fluxes and local events, may be responsible for microdomain $[Ca^{2+}]_i$ increase that either sensitizes RyRs for CICR or leads to direct RyR activation. Functional $InsP_3R$/RyR crosstalk can in principle operate in both directions. Hence, microdomain $[Ca^{2+}]_i$ elevations could sensitize $InsP_3Rs$ for $InsP_3$, which would favour $InsP_3R$ openings.[20] The effect has been shown in other cell types, whereby CICR was the coordinative mechanism of the concerted opening of clustered $InsP_3Rs$.[30] We increased the Ca^{2+} spark frequency with rapid and homogeneous photolytic $[Ca^{2+}]_i$ jumps. Ca^{2+} sparks occurring subsequently to this intervention provoked Ca^{2+} puffs in a coordinated fashion. It was suggested that $InsP_3R2$ open probability may be controlled with both $InsP_3$ and Ca^{2+}. Therefore, $InsP_3R2s$ with $InsP_3$ bound can be fully activated with additional Ca^{2+} binding.[9]

Physiological and pathophysiological implications

In atrial tissue collected from patients with atrial fibrillation, it has been reported that chronic pressure overload of the atrial wall is associated with increased $InsP_3R$ expression. Such an increase may be a likely contributor for the initiation or perpetuation of atrial fibrillation.[31] In functional studies performed in atrial cells from rabbit HF model, increased Ca^{2+} transients related to enhanced IP3ICR expression have been identified.[32] The TG model used in our study shows a mild up-regulation of $InsP_3R2$ expression with similarities in terms of cellular remodelling reported for human dilated cardiomyopathy with arrhythmogenic substrate.[4,13,14,31,33,34] The need for synergistic binding of $InsP_3$ and Ca^{2+} on the $InsP_3R$ for subsequent activation was supported by our Ca^{2+} uncaging experiments, where increased $[Ca^{2+}]_i$ was associated with an upregulated IP3ICR/CICR event ratio.[9] With increased intracellular $InsP_3$ concentrations, $InsP_3Rs$ might become activated at normal diastolic Ca^{2+} levels and therefore may promote arrhythmic Ca^{2+} transients in cardiac diseases with increased $InsP_3R$ expression.[9] In addition, functional $InsP_3R$ up-regulation may have positive inotropic consequences.[35] Although the number of directly observed $InsP_3R$/RyR crosstalk events was rather low in our hands, a significant impact on CICR/ECC is possible. The present study supports a modulatory role of $InsP_3R$/RyR crosstalk mechanisms for ECC and suggests IP3ICR as a potential target for treating Ca^{2+}-dependent cardiac disorders.

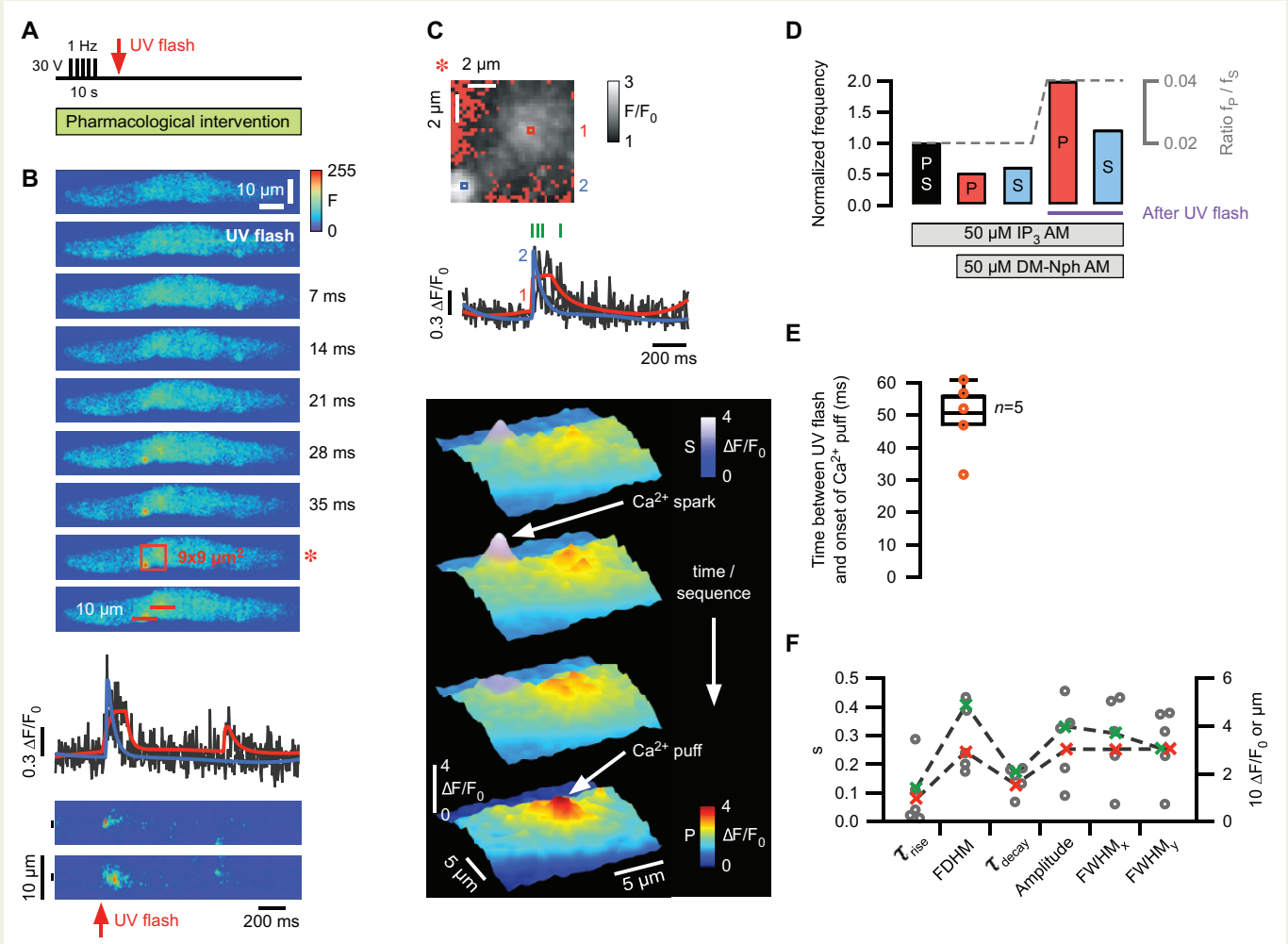

Figure 7 IP3ICR facilitated by local CICR. (*A*) Experimental protocol, cells incubated with 50 µmol/L $InsP_3$ AM and 50 µmol/L DM-nitrophen AM. (*B*) Time series of full-frame images with a Ca^{2+} spark and a Ca^{2+} puff, the red box and lines indicate the ROI and the position for pseudo-linescans extracted from image-series. The pseudo-linescans showing a coincidentally occurring Ca^{2+} puff (red) and Ca^{2+} spark (blue). (*C*) The ROI (red asterisk) is shown as a x-y-t projection of the SOI. The two Ca^{2+} release events are classified based on F/F_0 fluorescence of selected pixels from the ROI (green marks correspond to the surface plots). (*D*) Frequency ratio of Ca^{2+} puffs (f_P) and Ca^{2+} sparks (f_S) before and after photolytic $[Ca^{2+}]_i$ increase (50 µmol/L $InsP_3$ AM, 50 µmol/L DM-nitrophen AM). The ratio f_P/f_S raised from 0.02 to 0.04 due to CICR activity. (*E*) Time window between UV-flash photolysis and Ca^{2+} puff occurrence (49 ms, 12 SD). (*F*) Kinetic parameters from classified Ca^{2+} puffs ($n_e = 5$, $n_c = 5$, $N = 4$) with mean values (marked in red) were compared to previously obtained data for Ca^{2+} puffs ($n_e = 95$, marked in green; data extracted from *Figure 2* and Supplementary material online, *Table S1*). Selected data are presented as Tukey boxplot with median value.

Supplementary material

Supplementary material is available at *Cardiovascular Research* online.

Acknowledgements

The authors thank Ernst Niggli, Radoslav Janicek, Miguel Fernandez-Tenorio, and Ange Maguy for their helpful comments on the manuscript, Marianne Courtehoux for her expertise in immunocytochemistry and Ardo Illaste for software development.

Funding

This work was supported by the Swiss National Science Foundation (31003A-149301) and Novartis Res. Foundation to M.E. Funding to pay the Open Access publication charges for this article was provided by SNF.

Conflict of interest: none declared.

REFERENCES

1. Bers D. Cardiac excitation-contraction coupling. *Nature* 2002;**415**:198–205.
2. Zima AV, Blatter LA. Inositol-1,4,5-trisphosphate-dependent Ca^{2+} signalling in cat atrial excitation-contraction coupling and arrhythmias. *J Physiol* 2004;**555**:607–615.

3. Mackenzie L, Roderick HL, Proven A, Conway SJ, Bootman MD. Inositol 1,4,5-trisphosphate receptors in the heart. *Bio Res* 2004;**37**:553–557.
4. Harzheim D, Movassagh M, Foo RS-Y, Ritter O, Tashfeen A, Conway SJ, Bootman MD, Roderick HL. Increased $InsP_3Rs$ in the junctional sarcoplasmic reticulum augment Ca^{2+} transients and arrhythmias associated with cardiac hypertrophy. *PNAS* 2009;**106**:11406–11411.
5. Niggli E, Shirokova N. A guide to sparkology: the taxonomy of elementary cellular Ca^{2+} signaling events. *Cell Calcium* 2007;**42**:379–387.
6. Cheng H, Lederer WJ, Cannell MB. Calcium sparks: elementary events underlying excitation-contraction coupling in heart muscle. *Science* 1993;**262**:740–744.
7. Parker I, Yao Y. Regenerative release of calcium from functionally discrete subcellular stores by inositol trisphosphate. *Proc Royal Soci Biol Sci* 1991;**246**:269–274.
8. Horn T, Ullrich ND, Egger M. 'Eventless' $InsP_3$-dependent SR-Ca^{2+} release affecting atrial Ca^{2+} sparks. *J Physiol* 2013;**591**:2103–2111.
9. Kockskämper J, Zima AV, Roderick HL, Pieske B, Blatter LA, Bootman MD. Emerging roles of inositol 1,4,5-trisphosphate signaling in cardiac myocytes. *J Mol Cell Cardiol* 2008;**45**:128–147.
10. Bootman MD, Smyrnias I, Thul R, Coombes S, Roderick HL. Atrial cardiomyocyte calcium signalling. *Biochim Biophys Acta* 2011;**1813**:922–934.
11. Li X, Zima AV, Sheikh F, Blatter LA, Chen J. Endothelin-1-induced arrhythmogenic Ca^{2+} signaling is abolished in atrial myocytes of inositol-1,4,5-trisphosphate(IP_3)-receptor type 2-deficient mice. *Circ Res* 2005;**96**:1274–1281.
12. Nakayama H, Bodi I, Maillet M, DeSantiago J, Domeier T, Mikoshiba K, Lorenz J, Blatter L, Bers D, Molkentin J. The IP_3 receptor regulates cardiac hypertrophy in response to select stimuli. *Circ Res* 2010;**107**:659–666.
13. Harzheim D, Talasila A, Movassagh M, Foo RSY, Figg N, Bootman MD, Roderick HL. Elevated $InsP_3R$ expression underlies enhanced calcium fluxes and spontaneous extra-systolic calcium release events in hypertrophic cardiac myocytes. *Channels* 2010;**4**:67–71.
14. Sankar N, detombe PP, Mignery GA. Calcineurin-NFATc Regulates Type 2 Inositol 1,4,5-Trisphosphate Receptor ($InsP_3R2$) Expression during Cardiac Remodeling. *J Biol Chem* 2014;**289**:6188–6198.
15. Hohendanner F, Walther S, Maxwell JT, Kettlewell S, Awad S, Smith GL, Lonchyna VA, Blatter LA. Inositol-1,4,5-trisphosphate induced Ca^{2+} release and excitation-contraction coupling in atrial myocytes from normal and failing hearts. *J Physiol* 2015;**593**:1459–1477.
16. Bányász T, Chen-Izu Y, Balke CW, Izu LT. A new approach to the detection and statistical classification of Ca^{2+} sparks. *Biophys J* 2007;**92**:4458–4465.
17. Illaste A, Wullschleger M, Fernández-Tenorio M, Egger M, Niggli E. Extracting Detailed Ca^{2+} Signaling Information from Noisy Confocal Images. *Biophys J* 2014;**106**:532A–532A.
18. Ester M, Kriegel HP, Sander J, Xu X. A density-based algorithm for discovering clusters in large spatial databases with noise. *Proceedings of Second International Conference on Knowledge Discovery and Data Mining (KDD 96)*, E. Simoudis, J. Han, U. Fayyad, Eds. AAAI Press, Portland, Oregon, 1996;226–231.
19. Picht E, Zima AV, Blatter LA, Bers DM. SparkMaster: automated calcium spark analysis with ImageJ. *Am J Physiol* 2007;**293**:C1073–C1081.
20. Foskett JK, White C, Cheung K-H, Mak D-OD. Inositol trisphosphate receptor Ca^{2+} release channels. *Physiol Rev* 2007;**87**:593–658.
21. Escobar AL, Perez CG, Reyes ME, Lucero SG, Kornyeyev D, Mejía-Alvarez R, Ramos-Franco J. Role of inositol 1,4,5-trisphosphate in the regulation of ventricular Ca^{2+} signaling in intact mouse heart. *J Mol Cell Cardiol* 2012;**53**:768–779.
22. Signore S, Sorrentino A, Ferreira-Martins J, Kannappan R, Shafaie M, Del Ben F, Isobe K, Arranto C, Wybieralska E, Webster A, Sanada F, Ogórek B, Zheng H, Liu X, Del Monte F, D'Alessandro DA, Wunimenghe O, Michler RE, Hosoda T, Goichberg P, Leri A, Kajstura J, Anversa P, Rota M. Inositol 1,4,5-trisphosphate receptors and human left ventricular myocytes. *Circulation* 2013;**128**:1286–1297.
23. Wu X, Zhang T, Bossuyt J, Li X, McKinsey TA, Dedman JR, Olson EN, Chen J, Brown JH, Bers DM. Local $InsP_3$-dependent perinuclear Ca^{2+} signaling in cardiac myocyte excitation-transcription coupling. *J Clinic Invest* 2006;**116**:675–682.
24. Cooley N, Ouyang K, McMullen JR, Kiriazis H, Sheikh F, Wu W, Mu Y, Du X-J, Chen J, Woodcock EA. No contribution of IP_3-R2 to disease phenotype in models of dilated cardiomyopathy or pressure overload hypertrophy. *Circulation* 2013;**6**:318–325.
25. Bootman MD, Collins TJ, Mackenzie L, Roderick HL, Berridge MJ, Peppiatt CM. 2-aminoethoxydiphenyl borate (2-APB) is a reliable blocker of store-operated Ca^{2+} entry but an inconsistent inhibitor of $InsP_3$-induced Ca^{2+} release. *FASEB J* 2002;**16**:1145–1150.
26. Cheng H, Lederer WJ. Calcium sparks. *Physiol Rev* 2008;**88**:1491–1545.
27. Gordienko D, Bolton T. Crosstalk between ryanodine receptors and IP_3 receptors as a factor shaping spontaneous Ca^{2+}-release events in rabbit portal vein myocytes. *J Physiol* 2002;**542**:743–762.
28. Domeier TL, Zima AV, Maxwell JT, Huke S, Mignery GA, Blatter LA. IP3 receptor-dependent Ca^{2+} release modulates excitation-contraction coupling in rabbit ventricular myocytes. *Am J Physiol* 2008;**294**:H596–H604.
29. Ramay HR, Liu OZ, Sobie EA. Recovery of cardiac calcium release is controlled by sarcoplasmic reticulum refilling and ryanodine receptor sensitivity. *Cardiovasc Res* 2011;**91**:598–605.
30. Yamasaki Mann M, Demuro A, Parker I. Cytosolic [Ca^{2+}] regulation of $InsP_3$-evoked puffs. *Biochem J* 2013;**449**:167–173.
31. Yamda J, Ohkusa T, Nao T, Ueyama T, Yano M, Kobayashi S, Hamano K, Esato K, Matsuzaki M. Up-regulation of inositol 1,4,5 trisphosphate receptor expression in atrial tissue in patients with chronic atrial fibrillation. *J Am College Cardiol* 2001;**37**:1111–1119.
32. Hohendanner F, McCulloch AD, Blatter LA, Michailova AP. Calcium and IP3 dynamics in cardiac myocytes: experimental and computational perspectives and approaches. *Front Pharmacol* 2014;**5**:35.
33. Zhao Z-H, Zhang H-C, Xu Y, Zhang P, Li X-B, Liu Y-S, Guo J-H. Inositol-1,4,5-trisphosphate and ryanodine-dependent Ca^{2+} signaling in a chronic dog model of atrial fibrillation. *Cardiology* 2007;**107**:269–276.
34. Liang X, Xie H, Zhu P-H, Hu J, Zhao Q, Wang C-S, Yang C. Enhanced activity of inositol-1,4,5-trisphosphate receptors in atrial myocytes of atrial fibrillation patients. *Cardiology* 2009;**114**:180–191.
35. Bootman MD, Harzheim D, Smyrnias I, Conway SJ, Roderick HL. Temporal changes in atrial EC-coupling during prolonged stimulation with endothelin-1. *Cell Calcium* 2007;**42**:489–501.